geologicaacta

Citation: Corchete, V., 2026. Electrical conductivity inside Mars calculated beneath the InSight landing site.
Geologica Acta, 26.2, 1-pgs. DOI: 10.1344/GeologicaActa2026.24.2
Online ISSN: 1696-5728

Electrical conductivity inside Mars calculated beneath the InSight landing site

Victor Corchete

Higher Polytechnic School, University of Almeria
04120 Almeria, Spain. E-mail: corchete@ual.es

ABSTRACT

In a pioneer study, the electrical conductivity structure is determined beneath a fixed location on the Martian surface: the InSight landing site. The dataset used to attain this goal are the magnetic data recorded by InSight, from which are calculated the magnetic field variations in both high and low frequency, by spectral analysis. These variations are used to determine the surface ratios of vertical to horizontal magnetic field components, which are considered as the observed data that must be described/satisfied by some electrical conductivity models proposed. These models are the expression of the electrical conductivity structure of Mars, beneath the InSight landing site, and they should be recalculated when the data provided by future missions will be available (*e.g.* the Exobiology on Mars (ExoMars) Mission).

KEYWORDS | **Conductivity. Crust. Mantle. InSight Mission. Mars.**

INTRODUCTION

The Interior Exploration Using Seismic Investigations, Geodesy and Heat Transport (InSight) mission, landed on Mars in Elysium Planitia, has provided the first magnetic data measured at a fixed ground location on the Martian surface, through the InSight fluxgate magnetometer (IFG), which gives an invaluable opportunity to determine the Mars planet interior, from magnetic field based studies performed beneath this fixed location. From these data, InSight has made the first detection of magnetic pulsations on the Martian surface (Johnson *et al.*, 2020). These quasi-sinusoidal waves have been observed around midnight and in the late afternoon/early evening with periods from ~100s to a few minutes (Johnson *et al.*, 2020). These pulsations and the daily variation of the magnetic field joint to their harmonics, are time-varying magnetic fields that penetrate the subsurface to depths that depend on the interior electrical conductivity structure and the frequency content of these time variations. The Martian crust and mantle conductivities can be investigated using daily variations and their harmonics. For the investigation of the conductivities of the Martian crust, higher frequencies are required and it may be possible analysing the pulsations. Thus, the IFG data provides an unprecedented opportunity to investigate the interior conductivity structure of the Martian crust and mantle, beneath a fixed location beneath the Martian surface, which can be complementary to other investigations performed with satellite data (*e.g.* with satellite data from the Mars Atmosphere and Volatile Evolution (MAVEN) mission), to achieve the major InSight objective of determining the Martian interior structure.

DATA PREPARATION

The IFG data are the first dataset of direct measurements of time-varying magnetic fields on the Martian surface. Unfortunately, the presence of many gaps (very small and big gaps) in these data strongly limits their utilization in

magnetic field based studies, because the continue time-series of the magnetic field data are too short to study the long period variations: annual, seasonal and synodic solar rotation (~26-day period). Thus, the short period variations: daily variations, their harmonics and the pulsations, are the unique variations possible to study with the available IFG dataset. In the present study, five data series have been built from the IFG data (Supplement 1), from the IFG datasets with 2Hz sampling frequency (or 0.2Hz when the 2Hz data were not available for this date), selecting the data at a sampling rate of 0.02Hz to avoid the some small gaps that appear in data. The time series are initialized at the dates show in Supplement 1 as origin time, and finalized at the dates labelled as final time, when a big gap in data is found. Thus, the time series are built selecting the longest series of IFG data of continuous recording. They are the longer time-series available from all IFG dataset, and Figure 1 show these time series: the B_X (northward), B_Y (eastward) and B_Z (vertical-downward) components of the magnetic field versus time. The lower frequency data ($<10^{-3}$Hz) have been calculated through spectral analysis from these series (Figure 2; Bath, 1974; Brigham, 1988). The horizontal component of the magnetic field (B_H) is calculated in the frequency domain as $B_H=\sqrt{B_X^2+B_Y^2}$. Supplement 2 shows the daily period and its harmonics present in these low frequency data. The higher frequency

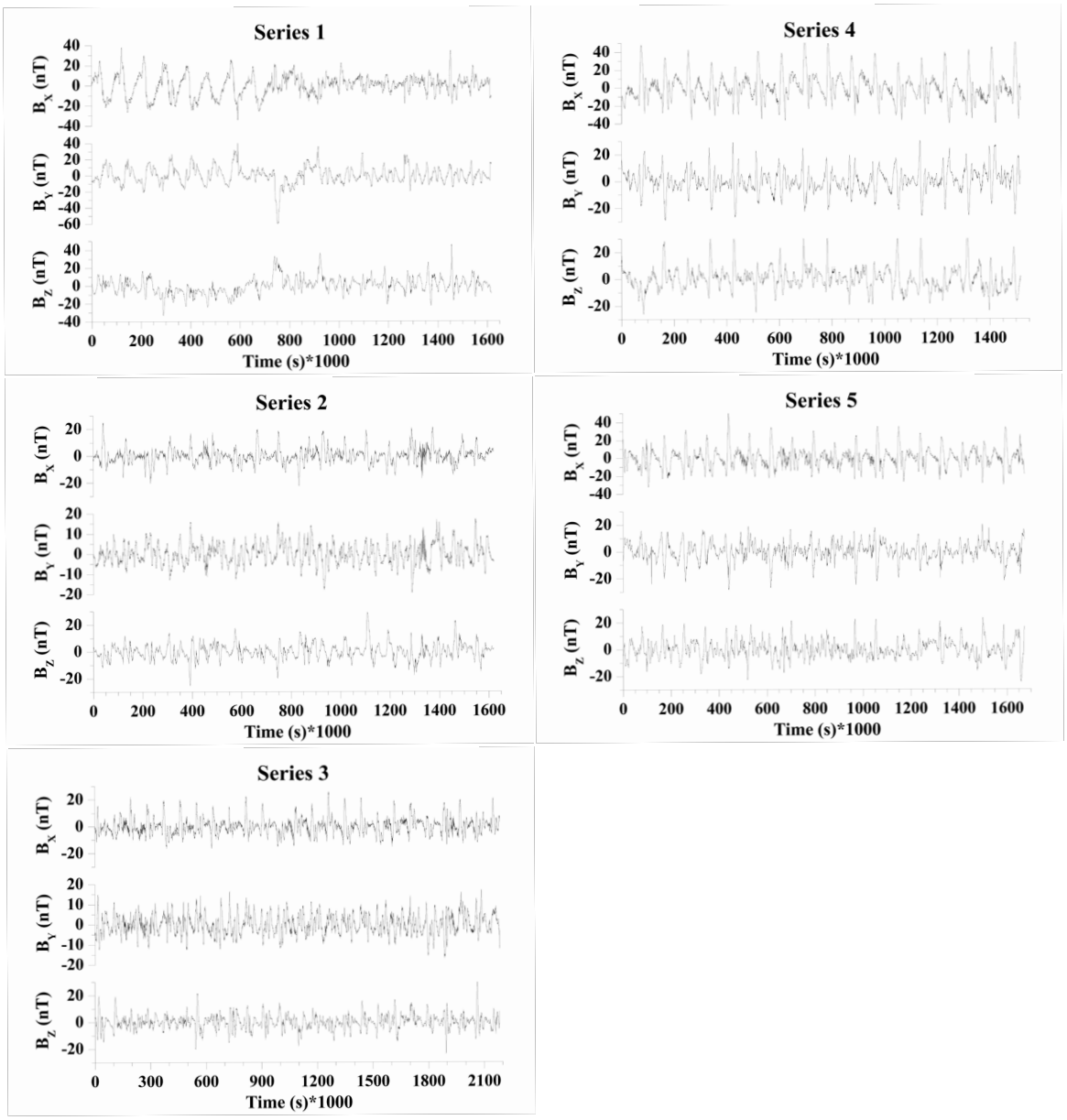

FIGURE 1. Data series listed in Supplement 1. The components of the magnetic field are represented without their respective mean. The time is given in coordinated universal time (UTC).

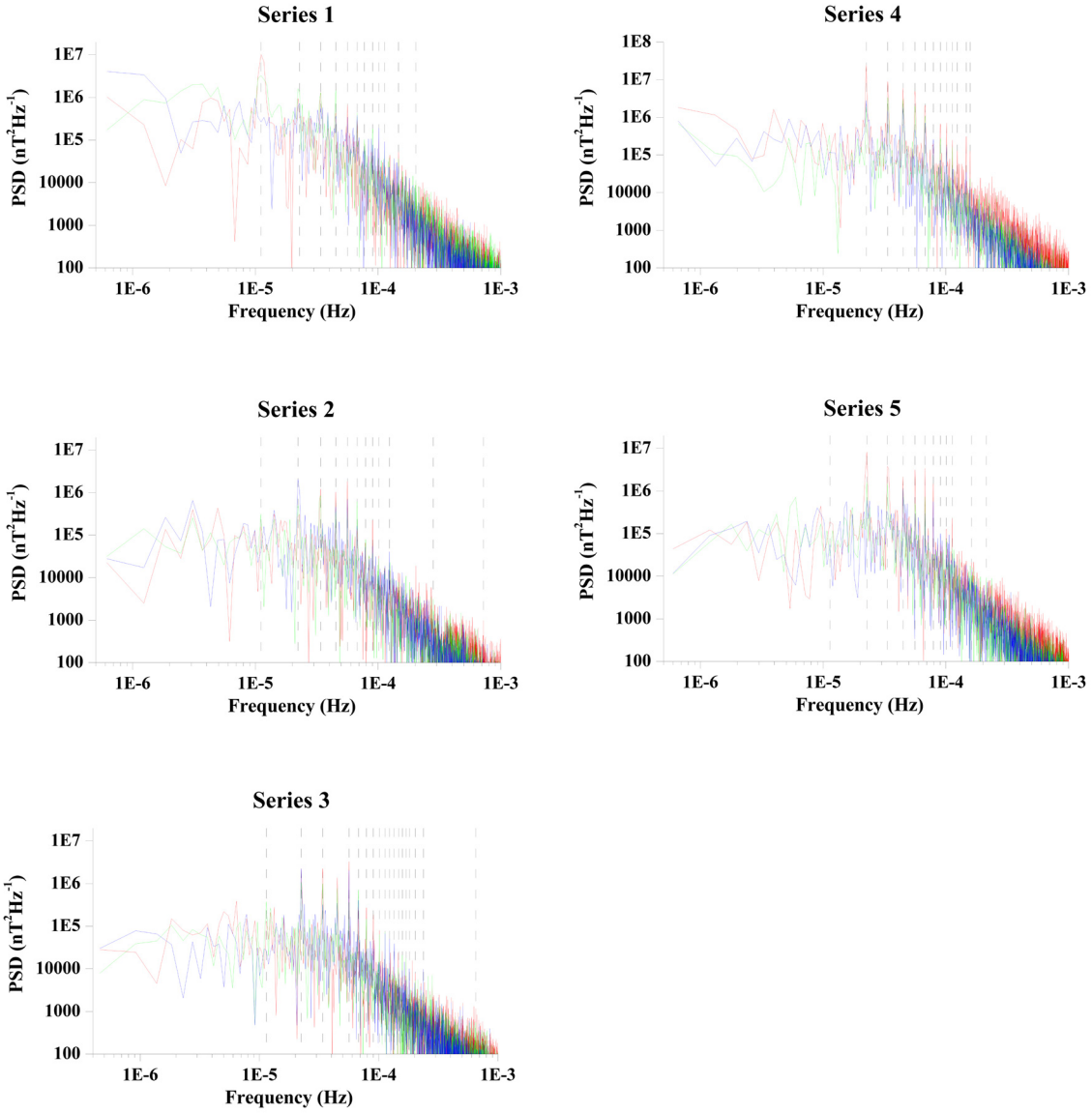

FIGURE 2. Power Spectral Density (PSD) calculated for the data series shown in Figure 1. The vertical black dashed lines correspond to the daily period and its harmonics. The components of the magnetic field are plotted with color lines (BX: red, BY: green, and BZ: blue).

data (>10^{-3}Hz) have been determined from the time records of the magnetic pulsations present in the IFG data, between the 0.9 sol and the 0.1 consecutive sol in Local Mean Solar Time (LMST, measured in decimal sol (sol is a Martian solar day= 88775s), from 0 to 1 sol), through spectral analysis of these time records (Supplement 3 and 4, and Figure 3). For both datasets: lower and higher frequency data, the frequencies are selected at clearly visible maxima of the amplitude spectra (Figure 2; 3; Supplement 3), other frequencies of the amplitude spectra are discarded because their amplitudes show a big scatter. Figure 4 shows the ratios $(B_Z/B_H)_{ob}$ determined in amplitude, where B_Z and B_H are the magnetic field components, vertical-downward and horizontal, respectively. These ratios have been calculated with the magnetic data shows in the Figure 2 and Supplement 3, and they are considered as the observed data of this study.

METHODOLOGY

The electrical conductivity of the crust and upper mantle can be determined comparing the observed data (Figure 4), with the theoretical response (the theoretical data) of electrical conductivity models, and considering the model that predicts the observed data with the minimum

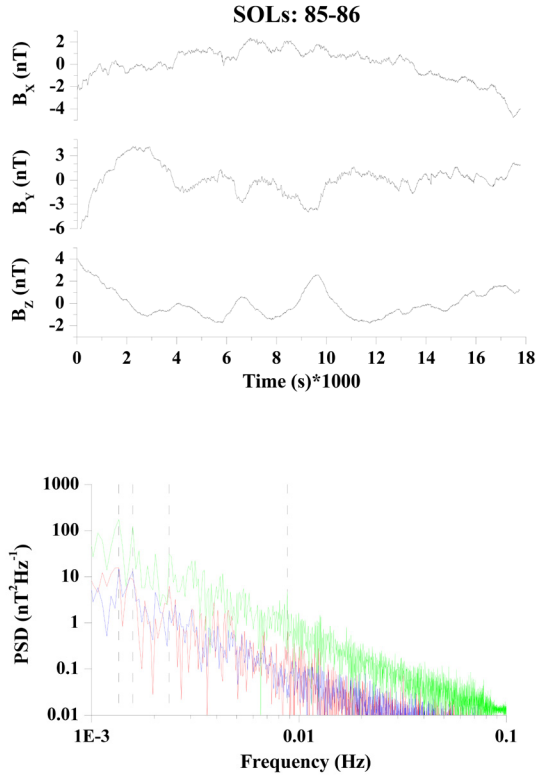

FIGURE 3. An example of the computation of the magnetic pulsation amplitudes for the time record corresponding to the sols: 85-86 (Supplement 4). The components of the magnetic field are represented without their respective mean. The vertical black dashed lines correspond to the periods (frequencies) of the magnetic pulsations (Supplements 3 and 4). The components of the magnetic field are plotted with color lines (BX: red, BY: green, and BZ: blue).

difference between both sets of data. Usually, these models consisting of spherical concentric shells of variable thickness and electrical conductivity (*e.g.* Banks, 1969; Khan *et al.*, 2011). Nevertheless, calculations made for plane and spherical conductors for frequencies from 10^{-8} to 1Hz, show that the planet curvature is not important for this frequency range (Srivastava, 1966). Thus, for the frequency range determined in this study (Figure 4), plane-stratified conducting models can be considered. These models will consist in N plane layers of variable thickness $d_{\square}$ and conductivity s_v with ν= 1, 2, … N. The last N-layer is extended to infinite (d_N= ∞). The theoretical surface ratios $(B_Z/B_H)_{th}$ (the theoretical data) are determined from the model by the expression

$$\left(\frac{B_Z}{B_H}\right)_{th}=¿(k)(1)$$

where i the imaginary unity, k is the wave number and T is the theoretical response of the conductivity model determined as described by Schmucker (1970). The wave number k is determined by

$$k=\sqrt{n(n+1)}/a(2)$$

where n take values from 1 to 5 and a is the Mars' radii (Srivastava, 1966), and the theoretical response T is calculated by

$$T(k)=\frac{k}{K_1 G_1(0)}$$

where K_v is given by

$$K_v=\sqrt{\frac{r+k^2}{2}}+i\sqrt{\frac{r-k^2}{2}}\ r^2=k^4+(4\pi\omega\sigma_v)^2\ \omega=2\pi f\ (f\ is\ the\ frequency)$$

and $G_1(0)$ is given by

$$G_v(z)=\frac{e^{-K_v z}-C_v e^{K_v z}}{e^{-K_v z}+C_v e^{K_v z}}(3)$$

where z is the depth beneath the medium surface, with z = 0 for the medium surface (*i.e.* for the planet surface), and C_v are determined from the continuity condition for the transient magnetic field vector at the interface $z= z_{v+1}$

$$K_v G_v(z_{v+1})=K_{v+1}G_{v+1}(z_{v+1})(4)$$
$$(z_1=0,\ z_2=d_1,\ \ldots,\ z_{v+1}=d_v+z_v,\ \ldots)$$

considering $G_N(z)$= 1 and using (4) as a recurrence formula. The theoretical data given by (1) are complex numbers, which will be evaluated in amplitude to be compared with the observed data determined also in amplitude. This comparison is numerically evaluated by the formula

$$\varepsilon=\sqrt{\frac{\sum_{i=1}^{M}\left[\left(\frac{B_Z}{B_H}\right)_{ob}-\left(\frac{B_Z}{B_H}\right)_{th}\right]^2}{M}}(5)$$

where M is the number of observed data, and the model that predicts the observed data with the minimum value of ε given by (5) is selected as final model.

RESULTS AND DISCUSSION

The observed data of higher frequencies (>10^{-3}Hz, Supplement 3) are firstly studied considering models

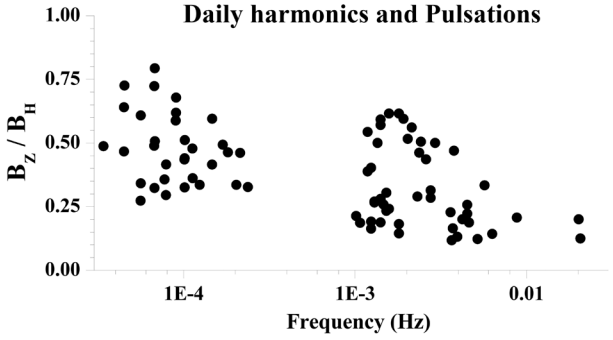

FIGURE 4. Surface ratios BZ/BH calculated from the magnetic field data shown in Figure 2 and Supplement 3.

consisting of only one semi-infinite layer (N= 1), with conductivity σ and the wave number k given by (2) with *n*= 5. The theoretical data are calculated by (1), and it is selected the model with minimum value of ε= 0.154416 given by (5), the model with σ= 1.59x10^{-3}S/m. Figure 5A shows the comparison between the observed data (pulsations) and the theoretical data calculated from this final model. Other values of *n* (from 1 to 4) are also computed, but these models show unrealistically very low values of σ, and they have been discarded. The values of the skin depth δ can be calculated for this final model and the frequency range of the observed data (Figure 4) by (Kuckes, 1973)

$$\delta = \sqrt{\frac{2}{\omega \mu_0 \sigma}}$$

where m_0 is the magnetic permeability of free space. If these values of δ ranges from 88 to 396km, and the crustal thickness beneath the InSight landing site is estimated in 32km (Smrekar *et al.*, 2019), it can be concluded that the observed data with the higher frequencies (>10^{-3}Hz) test the crust and uppermost mantle depths, but no observed data have been determined to test only the crustal depths. The crust and upper mantle conductivity structure also can be studied considering all frequency range of the observed data (Figure 4), computing now models with more layers. Figure 6 shows the model 1 considering two layers (N= 2 and *n*= 5) obtained with the best fit to the observed data (Figure 5B) and with ε= 0.139751, and the model 2 considering three layers (N= 3 and *n*= 5) fitting the observed data (Figure 5C) with ε= 0.139654. For the model 2, the first layer has been considered as the crust, with fixed values of thickness (32km) and conductivity (0.001S/m; Johnson *et al.*, 2020). The values of ε determined for the models shown in Figure 6 are very similar, concluding that both models can be

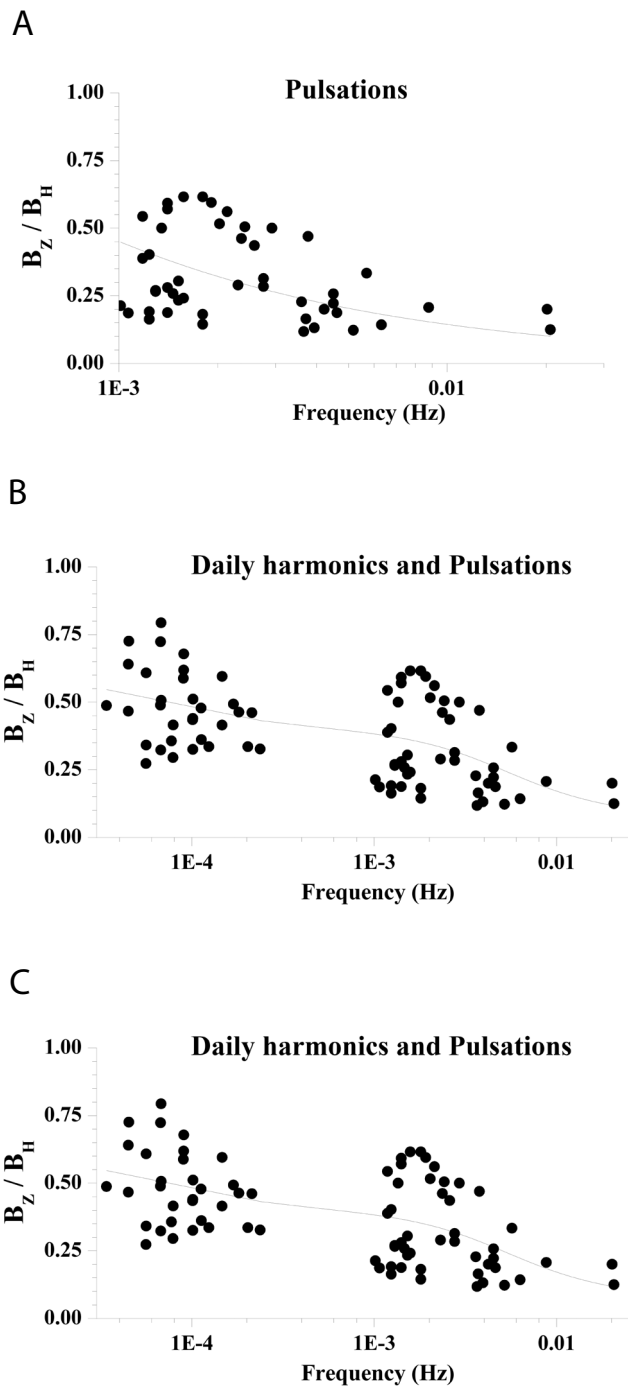

FIGURE 5. A) Observed surface ratios calculated from Supplement 3 and theoretical surface ratios determined by (1) for N 1 and n 5. B) Observed surface ratios shown in Figure 4 and theoretical surface ratios determined by (1) for N 2 and n 5. C) The observed surface ratios (b), and theoretical surface ratios determined by (1) for N 3 and n 5, with fixed values of thickness (32km) and conductivity (0.001S/m) for the first layer. The observed surface ratios are plotted as small black circles, and the theoretical surface ratios are plotted as continuous black line.

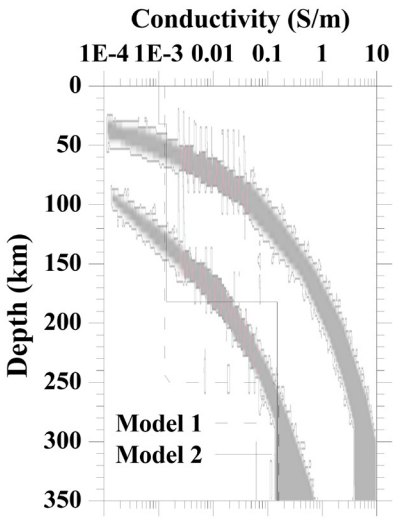

FIGURE 6. Electrical conductivity determined for the model 1 (N 2, dashed line): a layer with 250km-thick over a semi-infinite layer, and for the model 2 (N 3, continuous line): two layers (32 and 150km-thick) over a semi-infinite layer. The values of the minimum and maximum conductivity models, determined by Mocquet and Menvielle (2000), are drawn with dark gray areas for comparison.

considered valid as an interesting starting point for future investigations.

INTERPRETATION AND DISCUSSION

The electrical conductivity σ is an important geophysical parameter, because it represents a signature of the planet interior complementary to the seismic velocity, and can be used to know the Martian mantle temperature in the first 1000km-depth, because different composition models for the same temperature profile usually show similar electrical conductivity (Smrekar *et al.*, 2019). The theoretical studies of σ for the Mars interior (*e.g.* Mocquet and Menvielle, 2000; Vacher and Verhoeven, 2007) have shown how its values vary with key parameters of the mantle as temperature, composition or iron content, which are still not well constrained by the scarce available geochemical and geophysical data. The comparison of the present σ values (Figure 6) with other previous studies is very difficult to perform in detail, because this paper presents the first σ values inside Mars calculated just beneath the InSight landing site, and no previous studies of the Martian conductivity have been developed before just at this site. A comparison is only possible with previous global studies developed for all planet (*e.g.* Mocquet and Menvielle, 2000; Civet and Tarits, 2013, 2024), *i.e.* a comparison with spherical layer models with an average value of σ determined over all planet, for each spherical shell. These models generally show a very low resolution of layering for the depth range considered in the present study, *e.g.* Civet and Tarits (2013, 2014) determined σ distributions with depth considering layers with constant thickness of 200 and 180km-thick, respectively. In both distributions, it can be observed a discontinuity between the first and second layers (more clear in the results of Civet and Tarits (2013)), which coincides approximately in depth with the jump in σ shown in Figure 6. Also, in the σ distribution with depth determined for the mineralogy model of the Mars mantle proposed Bertka and Fei (1997), can be observed a pick in σ at 180km depth. According to this model, an olivine/wadsleyite phase transition could occur for the depth range, in which a rapid increase in conductivity values is determined. A more detailed comparison is only possible with the σ values determined by Mocquet and Menvielle (2000), who tested two mineralogical compositions of the Mars mantle: olivine-rich and pyroxene-rich, to obtain several hot and cold thermal profiles of electrical conductivity. They determined two σ distributions with depth (Figure 6, dark grey areas), and the results determined in the present study (Figure 6, black line) show a good agreement with their model of maximum conductivity above 100km depth, while those determined below 100km depth are in good agreement with their model of minimum conductivity.

CONCLUSIONS

A dataset of observed data is built from the InSight magnetic data, for the determination of electrical conductivity structure beneath the InSight landing site on Mars. From this dataset, two simple models of conductivity versus depth are computed, which are the first step in the knowledge of the Martian crust and mantle conductivity structure beneath the InSight landing site. It is particularly interesting to observe the good agreement between the σ values determined in the present study, and those determined by Mocquet and Menvielle (2000). However, the knowledge of the Martian crust and mantle electrical conductivity only will be improved, when more accurate magnetic data will be provided by future missions.

ACKNOWLEDGMENTS

The InSight mission has provided the data used in this study.

DATA AVAILABILITY STATEMENTS

The data used for this research are available from the Planetary Data System (PDS) of the National Aeronautics and Space Administration (NASA) at https://pds-geosciences.wustl.edu/missions/ insight/index.htm.

REFERENCES

Banks, R.J., 1969. Geomagnetic Variations and the Electrical Conductivity of the Upper Mantle. Geophysical Journal of the Royal Astronomy Society, 17, 457-487.

Bath, M., 1974. Spectral Analysis in Geophysics. Amsterdam, Elsevier, .

Bertka, C.M., Fei, Y., 1997. Mineralogy of the Martian interior up to core-mantle boundary pressures. Journal of Geophysical Research, Solid Earth, 102(B3), 5251-5264.

Brigham, E.O., 1988. The Fast Fourier Transform and Its Applications. New Jersey, Prentice Hall,

Civet, F., Tarits, P., 2013. Analysis of magnetic satellite data to infer the mantle electrical conductivity of telluric planets in the solar system. Planet and Space Science, 84, 102-111.

Civet, F., Tarits, P., 2014. Electrical conductivity of the mantle of Mars from MGS magnetic observations. Earth, Planets and Space, 66, 85.

Johnson, C.L., 22 others, 2020. Crustal and time-varying magnetics fields at the Insight landing site on Mars. Nature Geoscience, 13, 199-204.

Khan, A., Kuvshinov, A., Semenov, A., 2011. On the heterogeneous electrical conductivity structure of the Earth's mantle with implications for transition zone water content. Journal of Geophysical Research, 116, B01103. DOI:

10.1029/2010JB007458
Kuckes, A.F., 1973. Relations between electrical conductivity of a mantle and fluctuating magnetic fields. Geophysical Journal of the Royal Astronomy Society, 32, 119-131.
Mocquet, A., Menvielle, M., 2000. Complementarity of seismological and electromagnetic sounding methods for constraining the structure of the Martian mantle. Planetary and Space Science, 48, 1249-1260.
Schmucker, U., 1970. Anomalies of Geomagnetic Variations in the Southwestern United States. Berkeley, University of California Press, Bulletin of the Scripps Institution of Oceanography Series, 127-132,
Smrekar, S.E., 32 others, 2019. Pre-mission InSights on the Interior of Mars. Space Science Reviews, 215:3.
Srivastava, S.P., 1966. Theory of the magnetotelluric method for a spherical conductor. Geophysical Journal of the Royal Astronomy Society, 11, 373.
Vacher, P., Verhoeven, O., 2007. Modelling the electrical conductivity of iron-rich minerals for planetary applications. Planetary and Space Science, 55(4), 455-466.

Manuscript received July 2025;
revision accepted November 2025;
published February 2026.